N-Lobe Dynamics of Myosin Light Chain Dictates Its Mode of Interaction with Myosin V IQ1[†]

Irene Amata,[‡,⊥,#] Mariana Gallo,[‡,⊥] Matteo Pennestri,[‡] Maurizio Paci,[‡] Antonella Ragnini-Wilson,*[,§,||] and Daniel O. Cicero*

Department of Chemical Science and Technology, and Department of Biology, University of Rome "Tor Vergata", and Department of Cell Biology and Oncology, Consorzio Mario Negri Sud S.M. Imbaro, Italy

Received June 24, 2008; Revised Manuscript Received September 9, 2008

ABSTRACT: Myosin V motors regulate secretion and cell division in eukaryotes. How MyoV activity is differentially regulated by essential and calmodulin light chain binding remains unclear. We have used NMR spectroscopy to compare the dynamic behavior of Mlc1p, a budding yeast essential light chain, with that of the *Xenopus laevis* calmodulin. Both proteins have a similar structure and bind similar target proteins but differ in the mechanism by which they interact with the myosin V IQ1. This interaction is essential for MyoV activity. Here, we show that the rigid conformation of the loop connecting the two EF-hand motifs of the Mlc1p N-lobe explains its differential ability to interact with myosin V IQ1. Moreover, we show that the maintenance of the N-lobe structure is required for the essential function of Mlc1p *in vivo*. These data show that the core characteristics of myosin light chain N-lobes differentiate Mlc1p and calmodulin binding capability.

Cytokinesis is essential for cell division in all eukaryotes. This process involves coordination between membrane constriction driven by an acto-myosin II-based filamentous structure (called the actomyosin ring) and targeted membrane deposition driven by a myosin V motor. Myosin V captures organelles and/or secretory vesicles via its C-terminal globular tail domain (GTD[1]) thus promoting their delivery to the site of cytokinesis (*1*). In yeast, as well as in mammals, the function of both class II and class V myosins is regulated by the interaction of these intracellular motors with members of the EF-hand calmodulin superfamily of myosin light chains (*1, 2*). Calmodulin and myosin light chain act as master regulators of cytokinesis by binding in a calcium-regulated manner to the consensus sequence [IQXXXRGXXXR], termed the IQ motif, that is located in the neck domain of class II and class V myosins. In *Saccharomices cerevisiae*, the first myosin light chain discovered was yeast calmodulin (Cmd1) (*3*). Cmd1 acts as a regulatory light chain on the class V myosin Myo2p, to which also the essential myosin light chain 1 (Mlc1p) binds (*4*). Calmodulin and myosin light chain present the so-called EF-hand motif, formed by helix−loop−helix secondary structure elements, located in their N- and C-terminal lobes. Each lobe contains two EF-hand motifs. Figure 1 shows the multiple alignment of Mlc1p with yeast (Cmd1) and *Xenopus laevis* (CaM) calmodulins. In the figure, the N- and C-domains of the proteins and the topology, with the usual nomenclature, are indicated, and the EF-hand motifs are boxed. Ca^{2+} binding to EF-hands of myosin light chain is a well-known regulator of their interaction with IQ motifs. However, not all myosin light chains bind calcium (*5*−*7*). The fission and budding yeast essential myosin light chains SpCdc4p and ScMlc1p, although having a dumbbell shaped structure similar to calmodulin, are unable to bind calcium due to mutations in their EF-hand motifs. Interestingly, SpCdc4 and ScMlc1p in particular are essential light chains implicated in the regulation of cytokinesis (*4, 8, 9*).

The function of the budding yeast essential myosin light chain Mlc1p has been studied in detail by genetic and biochemical means. The results show that Mlc1p regulates different aspects of cytokinesis by binding to the actomyosin ring components, the class II myosin Myo1 and the IQGAP-like protein Iqg1/Cyk1, and to the vesicle and organelle motor class V myosin Myo2p. Mlc1p binding to the IQ motifs of Myo1p and Iqg1p is required for actomyosin ring contraction, while its binding to Myo2p is required for vesicle delivery to the mother-bud neck prior to and after actomyosin ring contraction. During cytokinesis, Mlc1p interaction with Myo1p, Myo2p, and Iqg1p must be timely and spatially coordinated to allow the formation of a septum separating the mother from the daughter cell, just after nuclear separation. Although several studies have addressed the question

[†] This work was supported by grant no. GGP 030341 from the Telethon Foundation, Italy.

* To whom correspondence should be adderessed. (A.R.-W. (for the mutagenesis studies)) Phone: +39 0872 570317. Fax: +39 0872 570412. E-mail:antonella.ragnini@uniroma2.it. (D.O.C. (for the NMR studies)) Phone: +39 06 7259 4835. Fax: +39 06 7259 4328. E-mail: cicero@scienze.uniroma2.it.

[‡] Department of Chemical Science and Technology.

[§] Department of Biology, University of Rome "Tor Vergata".

[||] Consorzio Mario Negri Sud S. M.

[⊥] Contributed equally to this work;

[#] Present address: EMBL Heidelberg, Meyerhofstrasse 1, 69117 Heidelberg, Germany.

[1] Abbreviations: Mlc1p, yeast myosin light chain 1 protein; CaM, animal calmodulins; Cmd1, yeast calmodulin; GTD, C-terminal globular tail domain; *ts*, thermo-sensitive phenotype; NOE, nuclear Overhauser effect; T_1, longitudinal relaxation time; T_2, transversal relaxation time; FRET, fluorescence resonance energy transfer; NMR, nuclear magnetic resonance; *J*, spectral density function.

10.1021/bi801178t CCC: $40.75
Published on Web 11/01/2008

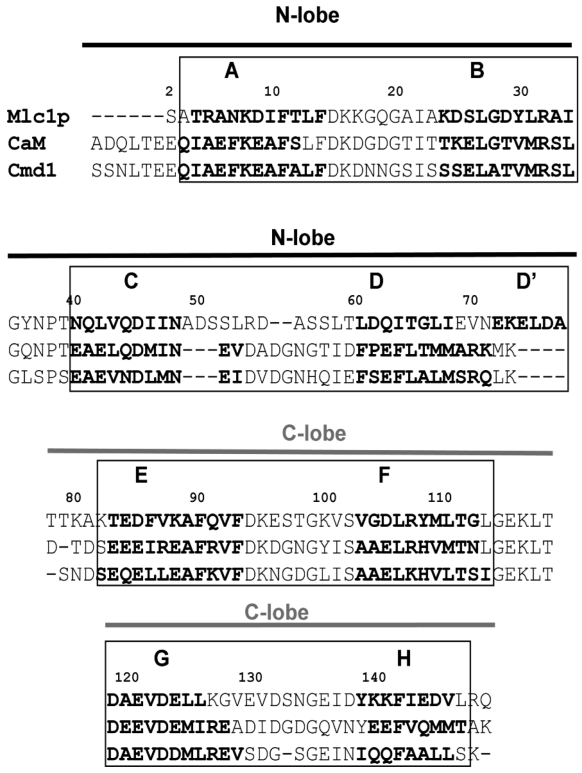

FIGURE 1: Topology and multiple alignment of yeast essential myosin light chain 1 (Mlc1p, Acc. number P53141), calmodulin from *Xenopus laevis* (CaM, Acc. number P62155), and yeast calmodulin (Cmd1, Acc. number P06787) proteins. The structure alignment was performed using the Dali Server, using the available structures (PDB entries: 2FCD and 2FCE, for the N-and C-lobes of Mlc1p, 1CFD for CaM, and 1LKJ for Cmd1). In bold are the residues in α-helical conformation, the nomenclature of the helices is indicated above (note that helix D′ is only present in Mlc1p). The four EF-hand motifs are coincident with the boxed regions, while at the top of the figure, the N- and C-lobes are shown in black and gray, respectively. The upper number refers to Mlc1p.

of how Mlc1p interacts with each target (*4, 9*−*11*), the mechanism by which Mlc1p coordinates these interactions remains unclear. In addition, it has not been clarified how the interactions of Mlc1p and Cmd1 with Myo2p IQ motifs regulate Myo2p function (*6, 7, 12, 13*). It has been proposed that the ability of Mlc1p to bind multiple targets during cytokinesis may be based on its ability to bind IQ motifs only with either the C-lobe or with both the N- and C-lobes (*6, 7, 12*). However, these aspects remain to be demonstrated. In particular, it remains to be established if the Mlc1p N-lobe can interact alone with a target.

In order to clarify how the structural differences of Cmd1 and Mlc1p might differentially regulate Myo2p activity prior to and after cytokinesis, we and others have previously undertaken a comprehensive study of the structures assumed by Mlc1p and Cmd1 when bound to each of the six IQ motifs forming the neck domain of Myo2p (*6, 7, 12*). These studies have shown that striking structural differences exist between Mlc1p and Cmd1 and that they differ in the way in which they interact with the same IQ1 motif of Myo2p. FRET analysis demonstrated that calmodulin interacts with Myo2p IQ1 using both the N- and C-lobes (*12*). In contrast, by using NMR we observed that only the Mlc1p C-lobe is involved in the interaction with Myo2p IQ1 motif (*7*). These findings have important implications for Myo2p function in vesicle/organelle binding and delivery to the site of cytokinesis. It has been shown in mammals that the myosin V MyoVa undergoes cycles of activation or inactivation upon Ca^{2+}-dependent calmodulin binding to IQ motifs (*1, 2*). The Ca^{2+}-calmodulin-dependent MyoV conformational changes lead to the interaction of MyoV C-terminal cargo binding domain (GTD) with its N-terminal-motor domain. It is still a matter of debate how MyoV GTD and the N-motor domain interact, nor is it clear which light chain is bound to IQ1 in the native MyoVa, LC-1sa, or calmodulin (*1, 2, 14*). Despite this, it has been observed that, when bound to IQ1 of MyoVa, the calmodulin C-terminal domain is part of, or is close to, the MyoV GTD-binding pocket. Thus, it is possible that calcium might regulate MyoV GTD and motor domain interaction by regulating the binding of calmodulin to IQ1 (*14*).

In the case of the yeast myosin V Myo2p, the ability to cycle between an active and an inactive state due to GTD and motor domain interaction has not been yet demonstrated. However, the high conservation of myosin V structure and function throughout evolution suggests that the yeast myosin V might also possess such properties (*15*). If this is the case, the ability of Mlc1p to bind with one lobe or of Cmd1 to bind with both lobes to IQ1 would have a clear effect on the ability of Myo2p to switch between an active and an inactive state.

The yeast calmodulin Cmd1 differs from the more thoroughly studied animal calmodulins (CaMs) in two important aspects. First, Cmd1 has only 60% identical residues when compared with sequences of CaMs isolated from vertebrates, scallops, and *Drosophila* (*16*−*18* see Figure 1). Second, the maximum binding number of Ca^{2+} to Cmd1 is 3 mol/mol, which is lower than that of vertebrate CaMs (4 mol/mol (*17*)). Despite this, to date, the interaction of vertebrate CaM with IQ motifs was studied by using IQ peptides derived from *S. cerevisiae* and the results extrapolated to Cmd1 (*12*).

In this work, we have used NMR spectroscopy to investigate the dynamic properties of Mlc1p and then compared it to that of CaM. We show that the Mlc1p N-lobe is more rigid than the C-lobe and that the IQ recognition mechanism is different for each one of these lobes. By comparing some of these features with the dynamic behavior of CaM, it is possible to explain the diverse mode of interaction of both proteins. Interestingly, we have observed that amino acids located within the N-lobe are required for Mlc1p function *in vivo*. Point mutations in amino acids located within the loop connecting the two EF-hands of the Mlc1p N-lobe cause thermo-sensitive defects in viability, cell separation, and the ability of Mlc1p to recruit Iqg1p to the mother-bud neck. How these mutations might result in structural or stability defects of Mlc1p is discussed.

EXPERIMENTAL PROCEDURES

NMR Sample Preparation. Uniformly ^{15}N-labeled samples of the Mlc1p protein were expressed and purified as previously described (*7*). A solution of 1.5 mM protein in 60 mM phospate buffer at pH 6.8, 0.33 M NaCl, 0.01% NaN_3, and 5% D_2O was initially prepared for the NMR relaxation analysis of Mlc1p. The sample was then diluted to protein concentrations of 0.4 mM (pH 6.8) and 0.8 mM (pHs 6.8 and 5.0) to study the concentration and pH dependency of the relaxation data.

NMR Spectroscopy. The NMR experiments were performed on Bruker Avance 700 and 400 MHz spectrometers equipped with pulsed field gradient triple resonance probes. The ^{15}N relaxation experiments were all measured at 25 °C. Measurements of ^{15}N T_1, ^{15}N T_2, and ^{15}N-{^{1}H} NOE were performed at 70.94 MHz ^{15}N frequency (1.5 mM, 0.8 mM, and 0.4 mM protein concentrations at pH 6.8, and 0.8 mM protein concentration at pH 5.0) and 40.57 MHz ^{15}N frequency (1.5 mM protein concentration at pH 6.8) using standard pulse schemes (*19, 20*). Six time points were collected for ^{15}N T_1 and ^{15}N T_2 in an interleaved manner. At 700 MHz, the ^{15}N T_1 delays used were of 14, 350, 700, 1050, 1400, and 2100 ms, and of 8.4, 25.1, 41.9, 75.4, 125.7, and 167.6 ms for ^{15}N T_2. At 400 MHz, delays of 28, 341, 677, 1013, 1350, and 1686 ms, and of 8.3, 33.1, 66.2, 99.3, 132.4, and 165.4 ms were used for ^{15}N T_1 and ^{15}N T_2, respectively.

In the direct dimension (^{1}H), the carrier frequency was set on the water resonance with a spectral width of 16.0 ppm; the indirect (^{15}N) dimension was centered at 116.8 ppm with a spectral width of 25 ppm. Two thousand complex data points with 256 complex increments were collected. Typical T_1 experiments were acquired with 64 scans and a repetition delay of 3 s. ^{15}N-{^{1}H} NOE spectra, both saturated and nonsaturated pairs, were acquired with 64 scans in an interleaved manner, employing a net relaxation delay of 4 s for each scan in both experiments.

NMR data were processed with NMRPipe (*21*) and analyzed with NMRView (*22*) programs on a Linux workstation. Spectra were zero filled to 4K and 512 points in the t_2 and t_1 dimensions, respectively, and were apodized using a phase-shifted Gaussian function.

Data Analysis. The chemical shifts assignment of ^{15}N and ^{1}H nuclei of Mlc1p was already available (*23*). The extraction of the relaxation parameters from the acquired spectra was achieved for more than 90% of the residues. Values of ^{15}N T_1 and ^{15}N T_2 parameters were calculated by fitting the measured peaks intensities to a single exponential decay curve. The ^{15}N-{^{1}H} NOE values obtained were corrected due to incomplete magnetization recovery during the relaxation delay in the experiments considering a nonselective ^{1}H longitudinal relaxation time of the protein (T_1) of 1.6 s by using the following equation (*24*):

$$NOE = (1 - a)NOE_m/(1 - a \times NOE_m)$$

where $a = \exp(-T/T_1)$, NOE_m is the measured ratio of intensities with and without ^{1}H irradiation, and T is the recovery delay between scans. Values of the steady-state ^{15}N-{^{1}H} NOE were established from the ratio of peak intensities obtained from spectra acquired with and without proton saturation. Data were fitted using the Rate Analysis routine of NMRView (*22*). The uncertainties of peak intensities were evaluated as the standard deviation of the spectral noise measured in a region free of crosspeaks. The ^{15}N-{^{1}H} NOE values were determined by the ratio of peak volumes of spectra recorded with and without ^{1}H saturation. Typically, errors were about of 2% for ^{15}N T_1 and T_2, and 5% for ^{15}N-{^{1}H} NOE measurements.

The Mlc1p relaxation data measured at 700 MHz and 25 °C for a solution containing 1.5 mM protein at pH 6.8 were deposited in the BRMB by updating the accession number 6332, which contains the Mlc1p chemical shift assignment in the same experimental conditions (*23*).

Analysis of ^{15}N relaxation data of Mlc1p using the spectral density mapping analysis (*25*) was performed according to the following equations:

$$\sigma_{NH} = (1/T_1)(\text{NOE-1})\gamma_N/\gamma_H$$

$$J(0) = (6/T_2\text{-}3/T_1\text{-}2.72\sigma_{NH})/(3d^2+4c^2)$$

$$J(\omega_N) = (4/T_1\text{-}5\sigma_{NH})/(3d^2 + 4c^2)$$

$$J(0.87\omega_H) = (4\sigma_{NH})/(5d^2)$$

where $d = (\mu_0 h\gamma_N\gamma_H/(8\pi^2))/\langle r^3_{NH}\rangle$, $c = \omega_N(\sigma_\theta - \sigma_\perp)/3^{1/2}$, μ_0 is the permeability of free space, h is the Planck's constant, γ_H and γ_N are the gyromagnetic ratio of ^{1}H and ^{15}N, respectively, $r_{NH} = 1.02$ Å is the average amide bond length, and $(\sigma_\theta - \sigma_\perp) = -160$ ppm is the chemical shift anisotropy for ^{15}N nuclei.

Isotropic Correlation Time Calculations. The following equations for the calculation of ^{15}N T_1, T_2, and ^{15}N-{^{1}H} NOE were used to calculate the correlation times of the two lobes, considering an isotropic tumbling and using only data from residues belonging to the helices of the N-lobe (7−14, 24−34, 40−48, 61−70, 72−77) or the C-lobe (84−91, 103−109, 119−126, 139−147):

$$1/T_1 = d^2[J(\omega_H - \omega_N) + 3J(\omega_N) + 6J(\omega_H + \omega_N)] + c^2J(\omega_N)$$

$$1/T_2 = 0.5d^2[4J(0) + J(\omega_H - \omega_N) + 3J(\omega_N) + 6J(\omega_H) + 6J(\omega_H + \omega_N)] + 1/6c^2[3J(\omega_N) + 4J(0)]$$

$$NOE = 1 + (\gamma_H/\gamma_N)d^2[6J(\omega_H + \omega_N) - J(\omega_H - \omega_N)]T_1$$

where d and c have the same definitions as those described above. If isotropic tumbling is considered, a single correlation time, τ_c, describes the overall motion of the object (the entire protein, or the single lobe, as in this case). In these conditions, the spectral density function can be expressed as (*26, 27*):

$$J(\omega) = S^2\tau_c/[1 + (\omega\tau_c)^2] + (1 - S^2)\{\tau'/[1 + (\omega\tau')^2]\}$$

with

$$1/\tau' = 1/\tau_c + 1/\tau_f$$

where τ_f is the local correlation time for fast motions. If only residues of structured regions are considered, S^2, which is the generalized order parameter describing the amplitude of the fast internal motion, can be considered constant and equal to 0.85, and $\tau_f = 0$ (*28*).

Using the relaxation data acquired for Mlc1p at pH 6.8 at different protein concentrations and at pH 5.0 for the 0.8 mM solution, the correlation time for each residue of the helices was calculated using the aforementioned equations, considering either T_1 and ^{15}N-{^{1}H} NOE, the T_1/T_2 ratio, or the T_1 alone (see text).

Anisotropic Calculations. The relaxation due to the dipole−dipole interaction between two nuclei in rigid molecules undergoing rotational Brownian motion in a general case of anisotropic tumbling are described by the following autocorrelation ($C(t)$) and spectral density ($J(\omega)$) functions (*29*):

$$C(t) = \sum_{n=1}^{5} C_n e^{-1/\tau_n}$$

$$J(\omega) = \sum_{n=1}^{5} C_n \frac{\tau_n}{1+\omega^2\tau_n^2}$$

where τ_n values are the effective correlation times, and C_N values are appropriate coefficients. In the case of Mlc1p, calculation of the rotational diffusion tensor (D) allowed us to simplify these equations because an axially symmetric rotational diffusion tensor can be described by two terms $D_{||}$ and $D_{\perp}$. In this case, the model-free spectral density function is given by (*30*):

$$J(\omega) = \frac{2}{5}\sum_{J=0}^{5} A_J \left[\frac{S^2\tau_j}{1+\omega^2\tau_j^2} + \frac{(1-S^2)\tau_J'}{1+\omega^2\tau_j'^2}\right]$$

where $\tau_j^{-1} = 6D_{\perp} - j^2(D_{\perp} - D_{||})$, $A_0 = (3\cos^2\theta - 1)^2/4$, $A_1 = 3\sin^2\theta\cos^2\theta$, $A_2 = (3/4)\sin^4\theta$, the angle between the unique axis of the diffusion tensor and the equilibrium orientation of the $\mu(t)$ vector is θ, $\tau_j' = (1/\tau_j + 1/\tau_e)^{-1}$, and ρ_e is the internal correlation time for motions of the considered internuclear vector in a molecular reference frame. The angle θ was calculated by using the module DIFFC of the DASHA software (*31*) and considering the X-ray structure of the Mlc1p-IQ4 complex structure (pdb entry 1M46). The C-lobe conformation was replaced by the free structure calculated previously (*7*). Finally, the DASHA software was used to calculate the expected T_1/T_2 ratios for each amide nitrogen belonging to residues of the four principal helices of the N-lobe.

Global Internal Motion Model. The extended spectral density function equations can account for the existence of three internal motions of proteins, namely, the global tumbling with correlation time t_c the fast motions, with correlation time t_f, and intermediate motions, with correlation time ρ_s (*32, 33*). The spectral density function then takes the following form:

$$J(\omega) = S^2\tau_c/[1+(\omega\tau_c)^2] + (S_f^2 - S^2)\tau_s'/[1+(\omega\tau_s')^2] + (1 - S_f^2)\tau_f'/[1+(\omega\tau_f')^2]$$

where $\tau_s' = \tau_s\tau_c/(\tau_s + \tau_c)$, $\tau_f' = \tau_f\tau_c/(\tau_f + \tau_c)$ and $S^2 = S_f^2S_s^2$.We have applied this model as done before by Tjandra et al. for CaM (*28*). In this way and using only residues with heteronuclear ^{15}N-{^{1}H} NOE > 0.6 that do not show significant internal motions in the ps time scale, we can consider $S_f^2 = 0.85$ and $\tau_f = 0$. Moreover, as the intermediate motion refers to the entire motion of the lobe, the parameters S_s^2 and τ_s are the same for all residues. This leaves, together with τ_c, only three variables to be calculated by fitting by minimizing the difference between calculated and observed relaxation data.

Media, Strains, Growth Conditions, and Mutant Selection. YPD medium and synthetic selective (SD) medium contained 20 g/L glucose, and the desired amino acid(s) were used for yeast growth. YPD medium containing 200 mg/L G418 (Geneticin; GibcoBRL) was used for the selection of kanamycin resistant cells. The selection of *Ura*$^-$ cells (FOA selection) was performed on SD or SC plates supplemented with 1 g/L 5-FOA (Nalgene). Yeast, *E.coli* growth, transformation, DNA manipulation, and PCR reactions were performed as previously described (*9*). Mlc1 mutants selected after site-directed and random mutagenesis were assayed along with the isogenic *wt* strain for growth under various conditions as follows. These cells, grown as single colony on plates, were resuspended in 200 μL of the indicated YPD or selected medium in 96 well microtiter plates. Subsequently, the cells were replicated onto plates containing the desired growth medium and incubated for 2−4 days at the indicated temperature.

Random Mutagenesis of MLC1. Random mutagenesis of *MLC1* was performed *in vitro* using mutagenic PCR essentially as previously described (*34*). Briefly, the plasmid YCp111 *MLC1*(1) was cut with *Hin*dIII before use in the mutagenic PCR reaction. The primers used to amplify the *MLC1* locus were [MLC1/-28/*Xma*I/fw] and [M13forward]. To favor the mis-incorporation of nucleotides during the mutagenic PCR, the final concentration of dTTP and dCTP was 0.4 mM each, while the final concentration of dATP and dGTP was 0.08 mM each. A typical mutagenic PCR reaction further contained 0.25−0.50 μg/mL of digested template, 0.5 μM each primer, 1× polymerase buffer (Gibco BRL), 1.5 mM $MgCl_2$, 0.3 mM $MnCl_2$, and 0.05 U/μL Taq polymerase (Gibco BRL) in a final volume of 100 μL. The PCR cycling profile was 5 min 94 °C − 35× [45 s 94 °C − 30 s 55 °C − 75 s 72 °C], 10 min 72 °C, hold 4 °C. In order to create plasmids expressing the mutagenized alleles of *MLC1*, the product of the mutagenic PCR was cotransformed together with a 6.8 kb fragment of *Nde*I/*Bsu*36I-digested YCp111 *MLC1*(1) into RSY105−6A (*mlc1*Δ) cells carrying plasmid pRS289 that expresses the *URA3* and *MLC1* genes. Approximately 400 *LEU*$^+$ transformants were picked and subsequently plated on medium containing 5-FOA at 25 °C to select cells that had lost pRS289. 83% of the *LEU*$^+$ cells were able to grow on 5-FOA containing medium at 25 °C, indicating that they express a functional copy of *MLC1* from plasmid YCp111. Twenty-one of the transformants showed a reduced growth at 35 °C compared to cells carrying YCp111 *MLC1*(1).

The plasmids of these cells were isolated as described (Fujimura and Sakuma, 1993) and retransformed into RSY105-6A (*mlc1*Δ) cells carrying plasmid pRS289 (*URA3*, *MLC1*). After the loss of plasmid pRS289 in growth medium containing 5-FOA at 25 °C, the transformant strains carrying plasmids YPP1, YPP2, YPP3, YPP4, YPP12, YPP13, YPP14, YP17, and YPP19 showed a *ts* lethal phenotype at 37 °C, while RSY105-6A (*mlc1*Δ) carrying YCp111 *MLC1*(1) cells were viable at this temperature. Noteworthy, the cells carrying the YPP plasmids did not show a *ts* phenotype before the loss of pRS289. This indicates that the *ts* phenotype in cells that have lost pRS289 is due to a defect in the *mlc1* allele in plasmid YCp111 and not due to another defect in the YCp111 derivate. Furthermore, this shows that the mutant *mlc1* alleles do not confer a dominant *ts* phenotype in *mlc1*Δ cells carrying plasmid pRS289. Thus, the above-mentioned YPP plasmids express recessive *mlc1* alleles that confer a *ts* lethal phenotype. The sequence of the *mlc1* allele in plasmids YPP3, YPP4, YPP9, YPP12, and YPP14 was determined by sequencing (VBC Genomics, GmbH, A). To prove that a mutation in the *mlc1* allele causes the *ts* phenotype, the mutagenized portion of the *MLC1* locus or a part of it was used to replace the respective wild type sequence of *MLC1* in plasmid YCp111 *MLC1*(3). As expected, the plasmids containing the subcloned mutagenized *mlc1* allele conferred a *ts* phenotype when transformed in *mlc1*Δ cells.

Microscope Equipment. An Axioplan 2 microscope (Zeiss, CH) equipped with a 63× Plan Apochromat oil immersion objective, an optovar (1.0−2.5×), filter sets for fluorescein isothiocyanate (FITC; GFP pictures), CFP, YFP, rhodamine, differential interference contrast (DIC) optics, an HBO 100 W UV lamp (Osram), and a cooled CCD camera (Spot, Diagnostic Instruments Inc.) were used. Microscope and camera were controlled by MetaView version 4.1 software (Universal Imaging, Corp., U.S.A.). Pictures were processed with Photoshop 5.0 (Adobe Systems Inc.)

RESULTS AND DISCUSSION

Two Lobes of Mlc1p Differ in Their Intermolecular Interaction Properties. ^{15}N relaxation measurements provide a very powerful way to study the dynamical behavior of a protein in solution. Normally, concentrated protein samples are used to perform these measurements, in order to obtain more accurate data. However, high concentrations can induce intermolecular interactions that can have a significant influence on the final outcome, especially regarding the overall tumbling of the proteins or domains of the protein. The protein used in this study carries an extra segment at the N-terminus (amino acids with negative numbering) corresponding to the His-tag sequence, useful for the purification process, that was not possible to cleave (see below). ^{15}N relaxation times and the ^{15}N-{^{1}H} NOE were measured at 700 and 400 MHz (proton frequency) for a sample of Mlc1p at high concentration (1.5 mM) and at pH 6.8. ^{15}N T_1 and ^{15}N T_2 values measured at the two fields and at 1.5 mM concentration revealed different behaviors between the two domains. The N-lobe shows average values of T_1 and T_2 larger and lower relative to the C-lobe, respectively (Figure 2A, black curve). This result strongly suggests that, in these conditions, the N-domain presents a slower tumbling than the C-domain, despite the fact that they are constituted by a very similar number of amino acids. To analyze if this difference was due to an intrinsic dynamic characteristic of the two lobes or if it was dependent on the concentration of the sample, we measured the relaxation times at different protein concentrations. Figure 2A shows the T_1 and T_2 values measured at 700 MHz as a function of the residue number at 0.4 (blue), 0.8 (red), and 1.5 mM protein (black). N- and C-lobes of Mlc1p present a different dynamic behavior as a function of protein concentration. T_1 and T_2 relaxation times of the C-lobe seem to be less affected by the concentration of protein. In contrast, T_1 values of the N-lobe increase when the concentration of the protein increases, while T_2 values show an opposite tendency. This result indicates that the N-lobe motion slows down with the increase of the concentration, suggesting a propensity of intermolecular interactions for this lobe.

One possible source of such interactions is the presence of the His-tag sequence. The easiest way to estimate the impact of this region is to remove it by enzymatic digestion. However, any attempt to hydrolyze the N-terminal His-tag produced a large amount of proteolyzed protein. Analysis of the fragments indicated that most of the degradation occurred at the C-lobe (data not shown). In order to investigate the impact of the presence of the His-tag fragment on the propensity of the N-lobe to self-interact, we measured the relaxation times at a lower pH (pH 5.0). In this way, the

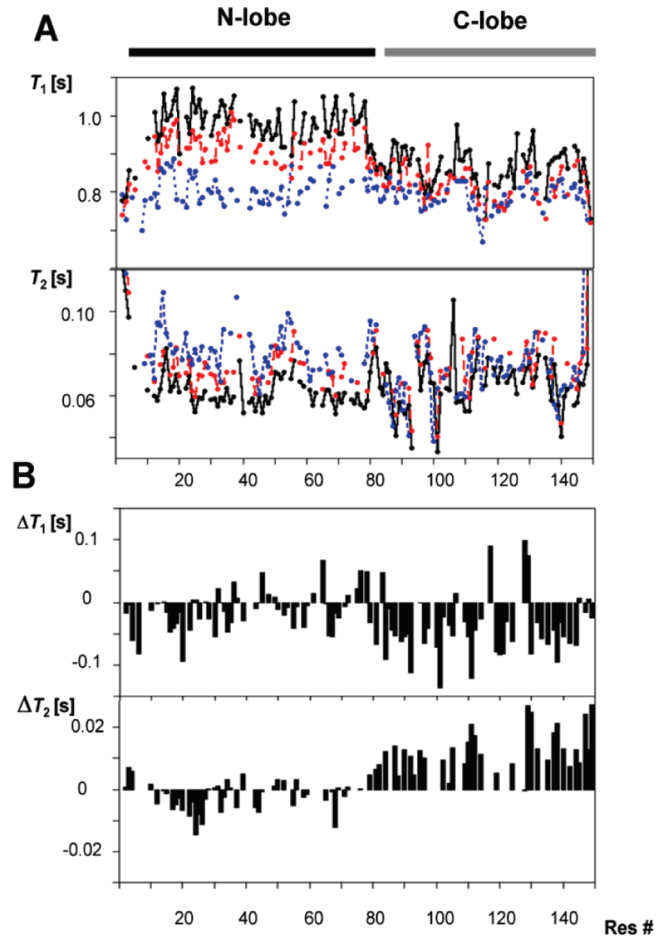

FIGURE 2: Dependence of the ^{15}N T_1 and T_2 relaxation times of Mlc1p on protein concentration and pH. (A) T_1 and T_2 relaxation rates of Mlc1p at pH 6.8 as a function of the residue number for 0.4, 0.8, and 1.5 mM protein concentrations (depicted in a blue, red, and black, respectively). (B) Difference of T_1 and T_2 relaxation rates of 0.8 mM Mlc1p as a function of the residue number between pH 6.8 and 5.0. The experiments were recorded at 25 °C and at 700 MHz proton frequency. In the upper part of the figure, regions corresponding to the N- and the C-lobes are indicated.

protonation of the histidine residues of the His-tag should produce an increase of the electrostatic repulsion between different His-tag segments. Thus, if the His-tag presence is responsible for the T_1 and T_2 trends observed for the N-lobe, at a lower pH we expected to find the same average hydrodynamical behavior for the two domains. However, we did not find large differences in the $\langle T_1 \rangle$ and $\langle T_2 \rangle$ for the N-lobe at pH 6.8 and 5.0 at 0.8 mM protein concentration (Figure 2B), and therefore, we excluded that the slower tumbling of the N-lobe was due to the presence of the His-tag. Interestingly, the C-lobe shows different behavior at pH 6.8 with respect to pH 5.0, with a decrease of $\langle T_1 \rangle$ and an increase of $\langle T_2 \rangle$ at the lower pH. In addition to this phenomenon, there are local changes in T_1 and T_2 rendering the more scattered data, a possible indication of conformational and/or dynamical changes internal to the lobe. The effect on the overall tumbling indicates that a low pH induces intermolecular interactions of the C-lobe. This incipient aggregation is probably due to the neutralization of negative surface charges in this lobe (Figure 3). In contrast, as the N-lobe presents a relatively less negative surface (Figure 3), it does not show relevant differential dynamic behavior at pH 6.8 and 5.0. Conversely, the N-lobe appears to have

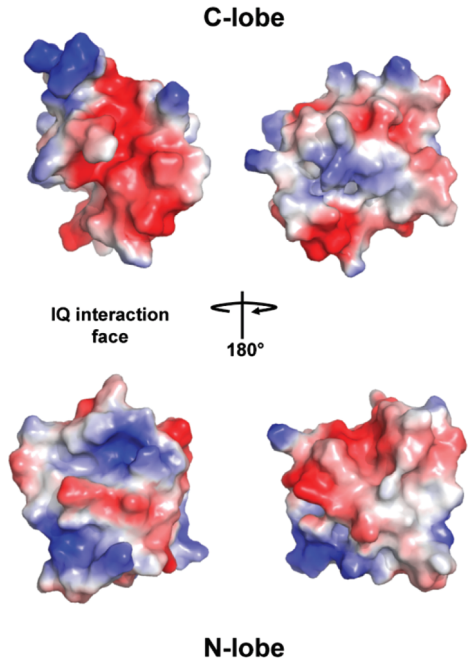

FIGURE 3: Potential energy surface of the N- and C-lobes of Mlc1p. The potential energy surface of the N- and C-lobes of Mlc1p (PDB entries 2FCD and 2FCE, respectively (*5*)) was calculated using the DelPhi/Grasp software (*35*) and visualized using the program PyMol (*36*). On the left, the face of the lobes interacting with the IQ motifs is shown, while on the right, a 180° rotation of the lobes is displayed.

greater tendency to aggregate at high concentrations and neutral pH than the C-lobe.

A convenient way to quantify the hydrodynamic properties of each lobe is to calculate the correlation times from the ^{15}N relaxation data using the Lipari−Szabo approach (*32, 33*). However, in the case of Mlc1p, the presence of two lobes moving independently, as in the case of calmodulin-like proteins, makes this calculation more difficult. The simplest model that considers each lobe as an isotropically tumbling module yields two apparent correlation times, one for each domain (*20, 28*). This value reflects a combination of two motions: the overall tumbling of the molecule and the global internal motion of the lobe.

Examination of the T_2 values, particularly those of the C-lobe, of Figure 2A, reveals that they show a very scattered behavior, with some residues showing lower than average values. This is a strong evidence for conformational exchange in the μs-ms time scale, that will be further characterized in the following section. This scattering prompted us to use only T_1 values for the correlation time calculations, as it was already done for Ca^{2+}-CaM (*20*) and CaM (*28*). To verify the validity of this approach, we calculated the correlation time for the N-lobe at 1.5 mM concentration exclusively considering residues belonging to the helices. Using T_1, T_2, and ^{15}N-{^{1}H} NOE data, we obtained a value of 11.3 ± 0.3 ns. When using the T_1/T_2 ratio, the calculated correlation time was 11.0 ± 0.4 ns, whereas the use of T_1 alone gave 10.8 ± 0.4 ns. A similar good agreement among the correlation time values obtained using different data sets was already observed for the analysis of CaM relaxation data (*28*). In contrast, the same calculation on the C-lobe gave more discordant values: 11.0 ± 1.5 ns (T_1, T_2,^{15}N-{^{1}H} NOE); 10.2 ± 1.0 ns (T_1/T_2), and 9.5 ± 0.5 ns (T_1), reflecting the contribution of the conformational exchange on the T_2 values.

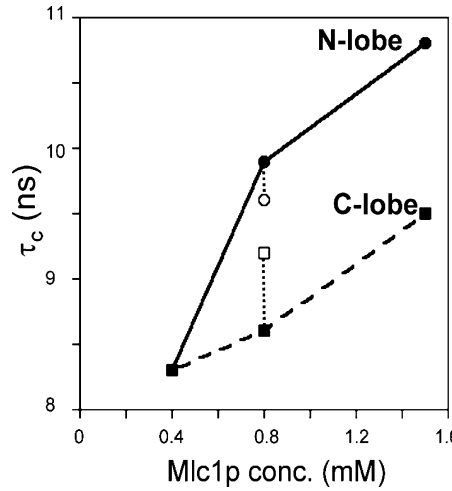

FIGURE 4: Correlation times for the Mlc1p N- and the C-lobes as a function of the protein concentration using the isotropic model and only T_1 data. Data determined at pH 6.8 are depicted as filled circles and squares for the N- and C-lobes, respectively, while data at pH 5.0 are illustrated as open circles and squares for the N- and C- domain, respectively.

The calculated correlation times using only T_1 values for the two lobes as a function of protein concentration are shown in Figure 4. The N-lobe shows a change of 2.5 ns in the apparent correlation time (from 10.8 to 8.3 ns) from 1.5 mM to 0.4 mM, whereas the C-lobe shows only a change of 1.2 ns (from 9.5 to 8.3 ns). This observation is in line with the fact that the N-lobe shows a larger tendency to self-aggregate at high concentrations. The C-lobe experiments mostly affect the global correlation time of the protein because of the fact that the two lobes are physically linked. At a protein concentration of 0.8 mM, the correlation time of the two lobes was calculated for two different pH values (6.8 and 5.0). As already discussed, the influence of pH on N-lobe tumbling is smaller than that observed for the C-lobe.

In summary, these results suggest that the N-lobe is involved in more significant intermolecular interactions at neutral pH conditions than the C-lobe. The presence of negative charges in the C-lobe prevents these interactions. In acidic conditions, the negative charges of the C-lobe are partially neutralized, and the C-lobe begins to be involved in intermolecular contacts. In a certain sense, these observations mirror the way Mlc1p interacts with the IQ motifs. The C-lobe is responsible for the electrostatic recognition of positively charged regions of Myo2p and experiments a large conformational change in order to form a channel that can accommodate the IQ helix (*7, 12*). However, the N-lobe only interacts through hydrophobic contacts of the surface of a rather compact and closed structure (*6, 12*). To date, there is no example of N-lobe interaction inducing a conformational change of this domain in Mlc1p. Two signals are known to provoke the opening of a lobe in the calmodulin superfamily: binding to divalent cations or phosphorylation. As was already discussed, Mlc1p cannot bind Ca^{2+}, and therefore, phosphorylation is the only posible alternative (*37*). However, although for the closely related SpCdc4p, phosphorylation of Ser 2 and 6 were observed *in vivo*, their role in protein function was excluded as mutation in these sites do not alter SpCdc4p activity or binding abilities (*38*). To our knowledge, the N-lobe of Mlc1p can interact only without any change in its conformation, and the observed

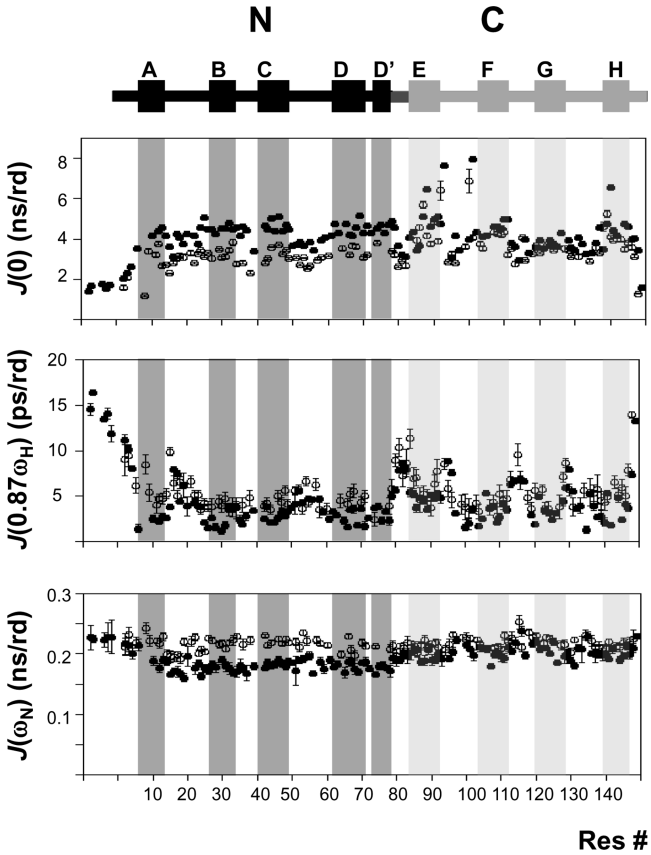

FIGURE 5: Reduced spectral density function analysis of Mlc1p relaxation rates at 700 MHz, calculated from data at 1.5 mM (●) and at 0.4 mM (○) both at pH 6.8 and 25 °C. Data relative to His-tag residues are labeled with negative numbers. Regions of secondary structure are indicated in the upper part of the figure and shadowed in the graphs. The N-and -C lobes are shown in black and gray, respectively.

self-association can be a measure of the tendency of the closed conformation to hydrophobically interact with possible targets. It is remarkable that the same effect was not detected for CaM or Cmd1, giving an indication of an enhanced superficial hydrophobicity of the N-lobe of Mlc1p.

C-lobe of Mlc1p Shows Enhanced Internal Mobility. We investigated the internal dynamics of Mlc1p using the reduced spectral density function mapping approach (*39, 40*). In this analysis, relaxation parameters are used to evaluate the spectral density functions $J(\omega)$ at selected frequencies. $J(\omega)$ represents the frequency distribution of rotational motions of N−H bond vectors, and it is a useful tool for discriminating the characteristic timescales of these motions. As this analysis does not require any assumption about the motion type, it is very valuable for direct comparisons of motion timescales between different proteins or different parts of the same protein.

$J(0)$, $J(0.87\omega_H)$, and $J(\omega_N)$ spectral density functions were calculated for Mlc1p at 1.5 and 0.4 mM and pH 6.8 (Figure 5). Similar distribution of the values was observed at both protein concentrations, thus excluding artifacts induced by the high concentration of protein at 1.5 mM. In particular, it can be noticed that values of $J(0)$ are higher at 1.5 mM than at 0.4 mM for the N-lobe, whereas the reverse is true for $J(\omega_N)$, which shows a decrease at higher protein concentration. This is consistent with a change in the correlation time of the N-lobe, which decreases in the case of a more diluted solution.

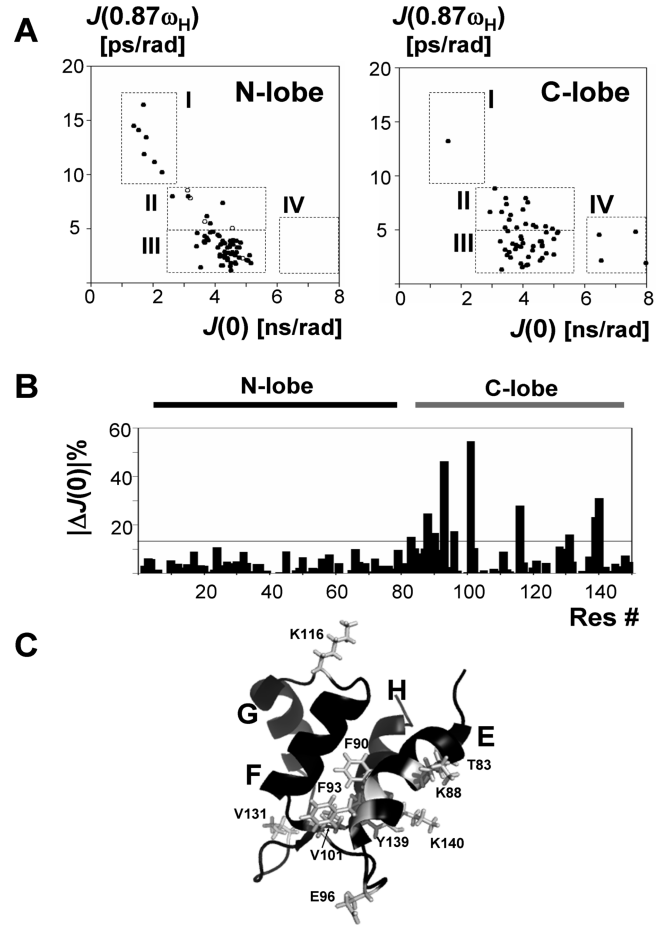

FIGURE 6: (A) Correlation plots between $J(0.87\omega_H)$ and $J(0)$ for the Mlc1p N-lobe (●) and the interdomain loop (the D-E loop, ○) (left panel) and of the C-lobe (right panel) (for the spectral density functions values, see Supporting Information). Four regions with different dynamics characteristics are evidenced (I, II, III, and IV; see text). (B) Percent of the relative difference between $J(0)$ (absolute value) for data acquired at 700 and 400 MHz, both measured for a 1.5 mM protein solution at pH 6.8 and 25 °C. The line in the graph indicates the average value plus a standard deviation. Residues over this value are subjected to slow conformational exchange phenomena. (C) Identified residues with slow conformational exchange contributions are mapped in the three-dimensional structure of the C-lobe of Mlc1p in light gray. The respective side chains are evidenced, and also, the helices are indicated.

In general, low $J(0)$ values are indicative of an increased internal mobility, as the N- and C- terminal ends of a protein and also flexible loops. In contrast, higher $J(0)$s are observed for the regions of secondary structure. However, enhanced values of $J(0.87\omega_H)$ reflect fast internal nano and picosecond motions with large high-frequency spectral densities, while regions of restricted mobility display lower $J(0.87\omega_H)$ values. Figure 5 shows that at least four residues of the C-lobe show larger than average values for $J(0)$, at both protein concentrations, indicating the possible presence of slow motions in the μs-ms time scale. At the same time, several residues of this lobe show larger than average values for $J(0.87\omega_H)$.

In Mlc1p, the observed trend for $J(0.87\omega_H)$ is effectively the opposite of that exhibited for $J(0)$. Figure 6A shows the correlation plot of $J(0)$ and $J(0.87\omega_H)$ for the two lobes of Mlc1p separately. This kind of graph is very useful because it emphasizes the regions of the protein with diverse dynamic behavior (*41*). We divided this plane into four regions with

different dynamical features. Residues belonging to the first region, with high $J(0.87\omega_H)$ and low $J(0)$ values, show highly uncorrelated internal motions, typical of very flexible residues. In fact, it includes residues S2 and A3 of the N-lobe, Q149 of the C-lobe, and His-tag residues. Region II involves residues presenting motions in the fast time scale. Residues of region III can be considered the structured core of the protein, as their ^{15}N relaxation properties do not show evidence of local mobility. In region IV, there are residues with low T_2 and, consequently, high $J(0)$ values (residues K88, F93, V101, and K140, all of them belonging to the C-lobe).

By analyzing the distribution of the mobility in the two lobes (Figure 6A), a significant difference can be noted between the two domains. The N-lobe presents a rather compact distribution of the points in region III, with the exception of residues S2, A3, and T4 (the unstructured N-terminal part) and K16 and K17 (belonging to the A−B loop). These residues show a significant degree of mobility, but all of the helices (A, B, C, D, and D′), as well as the loop of the second EF-hand motif (the C−D loop) and the loop connecting the two EF-hand motifs (the B−C loop), show no significant local mobility. The situation is very different for the C-lobe. In fact, the distribution of the residues in the graph is broader (right panel of Figure 6A). Together with the high mobility observed for the C-terminal Q149, local flexibility can be observed for most residues belonging to the two EF-hand loops and the loop connecting the two motifs. Four residues in region IV show a clear indication of μs-ms local movements; these residues belong to the first EF-hand motif. The presence of local mobility in the C-lobe, particularly in the μs-ms time scale, is a common feature of Mlc1p and CaM (*28*) and SpCdc4p (*42*), the other two proteins acting as myosin light chains and interacting with IQ motifs.

The comparison of the $J(0)$ values measured at two frequencies permits us to identify residues with exchange contributions to T_2 (*43*). Figure 6B shows the relative percent difference between $J(0)$ (in absolute value) calculated for data acquired at 700 and 400 MHz. Residues for which this difference is bigger than the average value plus a standard deviation are involved in slow conformational exchange phenomena. All of these residues belong to the C-lobe of Mlc1p and are mapped in the 3D structure in Figure 6C.

We interpret the differential internal mobility of the two lobes in terms of the mechanism of binding of Mlc1p. It was observed that the N-lobe does not significantly change its conformation when binding IQ2 or IQ3 (*7, 12*). However, the C-lobe undergoes a major conformational rearrangement upon binding the IQ motifs (*7*). The presence of mobility in the C-lobe, in particular on the first EF-hand and the link connecting the two motifs (the F-G loop), can be instrumental for the binding mechanism, as these regions, that must move to form the cavity for the IQ peptides, are those showing the largest flexibility. In this regard, the decrease in backbone flexibility upon IQ binding can be associated with a mechanism of enthalpy−entropy compensation (*44*), where the favorable hydrophobic interactions of the large binding surface can compensate for the loss in entropy caused by the quenching of internal motions.

Anisotropic Contribution to the ^{15}N Relaxation Rates. When considering the protein as a whole, we cannot rule out that the observed relaxation rates are to some extent influenced by an anisotropic tumbling. In solution, Mlc1p can populate a large number of conformations differing in the relative orientation of the two lobes due to the interdomain motion, as observed for CaM and Ca^{2+}-CaM (*20, 28*). This is caused by the flexibility of the linker connecting the two lobes, spanning residues 78−84. Those residues of the linker for which we have measured ^{15}N relaxation data are plotted as open circles in Figure 6A and show spectral density function values compatible with motions in the ps time scale, as they all belong to region II of the graph. One way to estimate to which extent this interdomain motion influences the overall tumbling of the molecule is to calculate the expected T_1/T_2 ratio for each helix in the N-lobe in a model with an extended rigid conformation and compare it with the experimentally observed value. A good model for the extended rigid conformation is the crystal structure of Mlc1p complexed with the IQ4 peptide (pdb 1m45) because in this structure, only the C-lobe is interacting with the peptide, and the N-lobe has no constraint that defines its orientation. This structure strongly resembles the dumbbell shape observed for Ca^{2+}-CaM in the crystal structure. Calculation of the diffusion tensor for this hypothetical rigid structure yields the following values for the three components: $D_{xx} = 9.641 \times 10^6$; $D_{yy} = 9.803 \times 10^6$; $D_{zz} = 2.433 \times 10^7$. To a good approximation, we can consider this molecule as a prolate ellipsoid, leading to an axial symmetry for the diffusion tensor with a ratio between the parallel and perpendicular components of 2.5.

Table 1: Predicted Average T_1/T_2 Ratio for Mlc1p N-Lobe Helices Assuming an Isotropic and an Anisotropic Model of Molecular Motion Compared with Experimental Values Recorded at 0.4 mM Protein Concentration

helix	T_1/T_2 iso	$\langle T_1/T_2 \rangle$ aniso	$\langle T_1/T_2 \rangle$ exp
A	10.1	11.2	9.8
B	10.1	13.7	10.3
C	10.1	12.3	10.6
D	10.1	13.9	11.2
all	10.1	12.8	10.5

If this structure were the only one to be present in solution, we would expect that NHs showing different angles with respect to the longer axis of the diffusion tensor will show very different T_1/T_2 ratios (*45*). Considering that in an α-helix the N−H bond vectors are parallel to the helix axis, with a rms deviation of about 15°, anisotropic tumbling will cause amides of a given helix to present very similar T_1/T_2 ratios. In contrast, amides in different helices will generally show different values, depending on the orientation of the helix axis relative to the anisotropic molecular diffusion tensor. Table 1 shows the calculated T_1/T_2 ratio average values for the four main helices of the N-lobe of Mlc1p considering the IQ4 complex structure and a correlation time for the N-lobe of 8 ns. The short D′ helix was not considered because we could measure the T_1/T_2 ratio only for one residue. For the dumbbell-shaped and rigid molecule, differences as large as 20% among the different helices can be expected. In contrast, the T_1/T_2 ratios measured at 0.4 mM protein (Table 1) show a more constant behavior, with a global mean value of 10.5 ± 1.2, very close to the estimated T_1/T_2 ratio for an isotropically tumbling molecule (10.1). This result clearly indicates the presence of a significant interdomain motion, which is key to its ability to bind the molecular

Table 2: Global Internal Motion for the N- and C-Lobes of Mlc1p and CaM

	N-lobe			C-lobe		
	τ_c [ns]	τ_s [ns]	S_s^2	τ_c [ns]	τ_s [ns]	S_s^2
Mlc1p	12.2	2.5	0.65	13.2	2.0	0.67
CaM[a]	12.8	2.8	0.66	10.6	2.8	0.66

[a] From Tjandra et al. (*28*).

targets using the two lobes. This large interdomain motion is so far a common characteristic of all the proteins belonging to the calmodulin superfamily.

Interdomain Motion Model. As Tjandra and co-workers have shown for CaM, it is possible to use the extended spectral density function to characterize motions of an entire domain of a protein (*28*). In this approach, a unique value for τ_s and S_s^2, the correlation time and generalized order parameter for slow internal motions, respectively, are considered for all residues within the domain. By exclusively using residues of structured regions of the protein, the helices, in the case of Mlc1p, one can safely consider that fast motions can be appropriately described by $S_f^2 = 0.85$ and $\rho_f = 0$. Therefore, the extended equation for the spectral density functions remains with only three variables to be fitted, namely, the overall correlation time (t_c), the correlation time (τ_s), and the order parameter (S_s^2) for the slow motion of the entire domain. ^{15}N relaxation data for Mlc1p obtained at 0.4 mM protein concentration were fitted, and the resulting parameters are presented in Table 2, along with the data obtained for CaM (*28*). This model suggests for Mlc1p an overall correlation time, t_c, in the 12−13 ns range, with internal motions of the two lobes on a time scale of 2−2.5 ns. In this way, the two time scales of the movement affecting the relaxation of nuclei within a lobe are separated, and the meaning of an isotropic tumbling of 8 ns as being the combination of a global tumbling of 13 ns and an internal motion of 2.5 ns is more clear.

The observed value for $S_f^2 = 0.66$ can be interpreted assuming a restricted diffusion of the individual domains in a cone. The value is compatible with an angle a of ∼30°, which is the same angle calculated for CaM (*28*), reinforcing the view of a very similar conformational behavior of the two myosin light chains.

Local Dynamics Differences between Mlc1p and CaM Are Closely Related to Their Differential IQ Interaction Mode. As was already discussed, the B−C loop of the N-lobe lacks significant internal motion in Mlc1p. The importance of this observation, and especially of residue N37, are more evident when comparing the dynamic behavior of apo-calmodulin (CaM) and Mlc1p. By using fluorescence resonance energy transfer techniques, it was observed that CaM binds IQ1 using both the N- and C-lobes (*12*). Subsequently, it was shown that Mlc1p binds IQ1 using only the C-lobe. This differential behavior has some structural basis already discussed (*7*). Here, we have investigated whether the N-domains belonging to Mlc1p and CaM show a different dynamical behavior that can additionally sustain the structural origin of their different IQ interaction. With this purpose, ^{15}N relaxation data measured by Tjandra et al. at 600 MHz proton frequency (*28*) were used to calculate the reduced spectral density functions for CaM from *Xenopus laevis* (the sequence and the structure alignment with Mlc1p and Cmd1 are shown in Figure 1). Correlation plots of $J(0.87\omega_H)$ vs $J(0)$ are shown in Figure 7A and B for CaM and Mlc1p, respectively. Different from Mlc1p, residues of the F−G loop of the C-lobe and of the B−C loop of the N-lobe and residues of the central loop of CaM (the D−E loop) are in region II of the plot, indicating significant mobility for these regions. In Figure 7A and B, the residues of the B−C loop are marked in black. Residue N42 of calmodulin shows a relevant local flexibility. In contraposition, the corresponding residue in Mlc1p, N37, is rather rigid. This local difference between the flexibility of residue N37 of Mlc1p and N42 of CaM is crucial in the binding processes of these two proteins with the IQ motifs. Figure 7C and D show the N-lobe structure of CaM and Mlc1p, respectively. Mlc1p presents an extra-helix D′ (residues 72−77), which is a unique feature of Mlc1p, not present in other proteins of the family (*7*). Residues of helix D′ make contacts that confer extra stability to the closed conformation of the N-lobe. As a consequence, the loop connecting the two EF-hand motifs in the N-lobe, the B−C loop, is very rigid with respect to all the other loops of the protein. In particular, residue N37 of this loop makes contact with the helix D′ by hydrogen bonding T78. This interaction contributes to the rigidity of the loop. In the case of CaM, as it does not present an equivalent of helix D′, the B−C loop (including residue N42) is not interacting with other parts of the protein and is much more flexible.

The flexibility (CaM) or rigidity (Mlc1p) of the B−C loop may be directly correlated with the ability of the two N-domains to interact with Myo2p IQ1. Mlc1p uses the N-lobe to interact only with IQ2 and IQ3, but not with IQ1 or IQ4 (*7, 12*). One important difference in the IQ sequence that explains the lack of N-lobe interaction is the presence of a Gly residue in IQ2 and IQ3, that is replaced by a Lys in IQ4 and an Ala in IQ1 (*7, 12*). In an eventual complex between these light chains and IQ1, an Ala residue would directly face the side chain of N42 (CaM) or N37 (Mlc1p) (Figure 8). The interaction between the IQ1 Ala side chain and the Asn residue of the light chain would force the latter to change its conformation. It is possible for CaM, which presents a flexible loop, to adapt itself in order to correctly interact with the IQ1 binding site (Figure 8A); but it is energetically less favorable for Mlc1p, which presents a rather rigid loop (Figure 8B), particularly due to the interaction with T78 of the D′ helix. No such interaction is present in CaM. Thus, the rigidity observed for the B−C loop of the N-domain leads to a differential binding mode of Mlc1p with IQ1, leaving the N-domain ready for interactions with a second molecular target.

Is the Compact Structure of the N-Lobe Required for Mlc1p Function in Vivo? A crucial question arising from this work is whether the residues that confer rigidity on the inter EF-hands loop, the B−C loop, are required for Mlc1p function *in vivo*. We made an attempt to answer this question by studying the effects of mutations in the B−C loop on Mlc1p function. A series of *mlc1* thermo-sensitive (*ts*) alleles defective in cytokinesis have been previously isolated using site-directed and random mutagenesis ((*9*) Ragnini-Wilson and Wagner, unpublished results; Figure 9). In all cases, the *mlc1 ts* alleles were expressed from the low copy plasmid YCp111 in cells lacking the genomic copy of MLC1 (*mlc1*Δ cells). Sequence analysis of the *mlc1 ts* mutants isolated by random mutagenesis showed that a number of them carry

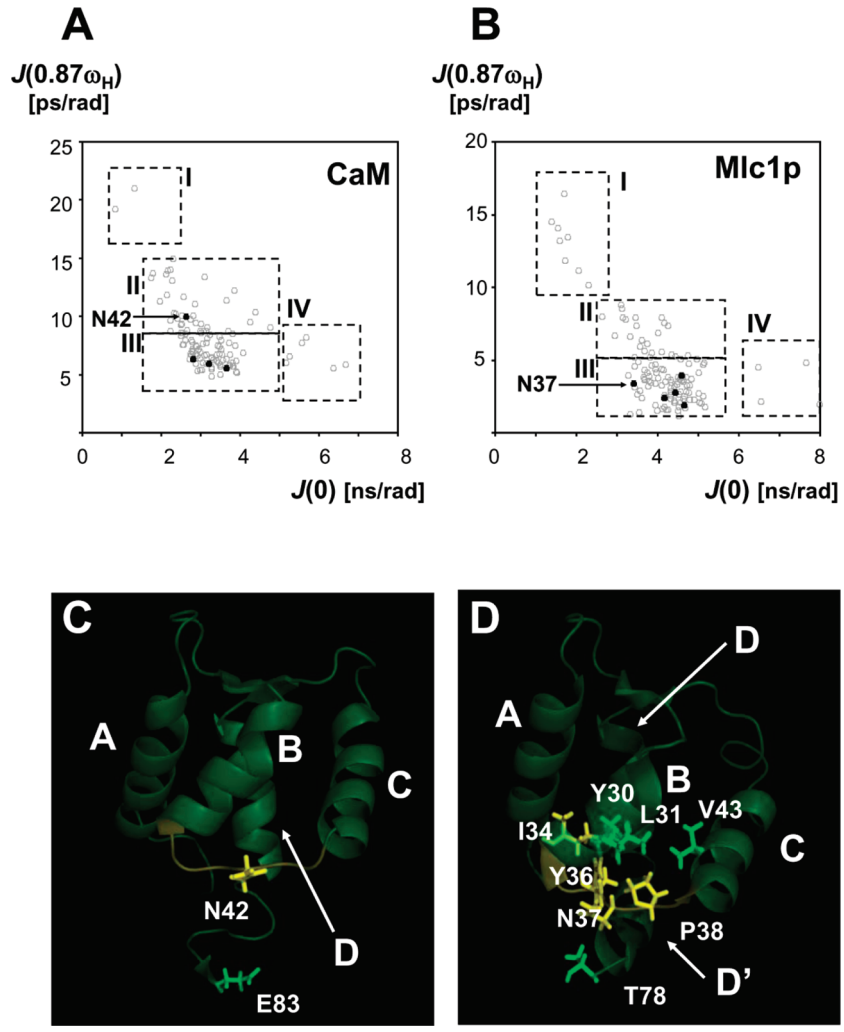

FIGURE 7: Comparison of dynamics of the loop inter EF-hand motifs, the B−C loop, of the N-lobe of CaM and Mlc1p. (A) Values of $J(0.87\omega_H)$ are plotted against the $J(0)$ values for each residue for calmodulin. Residues 40−44, belonging to the B−C loop, are in black. The four regions with different dynamics characteristics are also evidenced (see text). (B) The same for Mlc1p (residues 35−39, which correspond to the B−C loop, are depicted in black). (C) View of the N-lobe structure of CaM (PDB entry 1CFD) in a ribbon representation. The B−C loop is depicted in yellow. Side chains of residues N42 and E83 are evidenced, and the helices are indicated. (D) Ribbon representation of the N-lobe of Mlc1p (PDB entry 2FCD). The B−C loop is depicted in yellow. Side chains of residues N37 and T78, which are hydrogen bonded in Mlc1p and correspond to N42 and E83 in CaM, respectively, are evidenced. Side chains of residues that present relevant hydrophobic contacts that stabilize the loop in Mlc1p are also highlighted. The helices are indicated (note that helix D′ is absent in CaM).

single or multiple amino acid substitutions solely within the Mlc1p N-terminal domain (Table 3). Here we report the analysis of *mlc1−9, mlc1−14, mlc1−15*, and *mlc1−16*.

The mutant *mlc1−9* possesses four amino acid substitutions (Y36H, T39S, I47V, and D50E) located within the inter loops connecting the helices B−C (amino acids Y36H and T39S), the helix C (I47V), and in the C−D loop (D50E) of the Mlc1p N-lobe (Figure 7D). The *mlc1−14* allele carries a single substitution L59S that is located within the C−D inter loop of the second EF-hand of the N-lobe; the *mlc1−16* allele carries a valine to glycine substitution at position 43 (V43G) located within helix C. Interestingly, the *mlc1−15* allele carrying a substitution at position 34, (I34N) alone does not produce a detectable phenotype, but in combination with the C-terminal mutation Y139C (carried by the *mlc1−17* lethal allele) results in a *ts* phenotype (*mlc1−10* allele; Table 3). Generally speaking, a mutation of a residue in a protein can cause defects in the protein function either by altering the protein structure or by altering the nature of interaction with target proteins.

A general N-lobe structural destabilization might arise in the case of a substitution of valine 43 by glycine (V43G; *mlc1−16*), by substitution of isoleucine 47 by valine (I47V, *mlc1−9*), which are located in helix C, or when leucine 59 is substituted by serine (L59S; *mlc1−14*) located in the C−D loop because all of these amino acids participate together with L27 and K24 in the formation of a hydrophobic core that is essential for the correct packing of the two EF-hand motifs. The V43G (*mlc1−16*) mutation is expected to have an even more pronounced effect on N-lobe structure, as the glycine substitution of valine 43 is placed in the center of helix C. Thus, this group of mutations is likely to result in the destabilization of the Mlc1p N-lobe tertiary structure.

Mutation of threonine 39 by a serine residue (T39S) can be the cause of a defect in protein interaction. In the structure determined for the Mlc1p-IQ2 complex (*6*), the methyl group of T39 makes contact with the side chain of an asparagine residue of IQ2. However, the T39S mutation is found in the *mlc1−9* mutant together with other mutations that affect N-lobe structural stability, and thus, it is difficult to derive

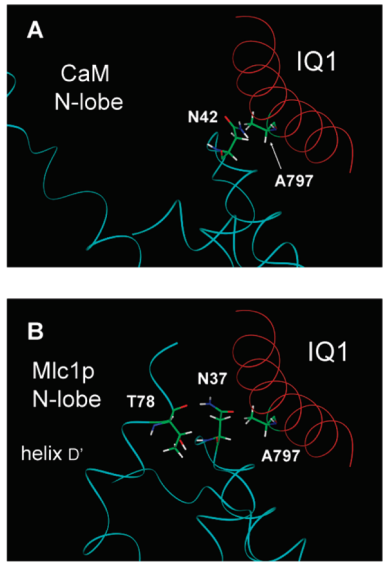

FIGURE 8: (A) Ribbon representation of a model of the complex of the N-lobe of CaM with IQ1, based on the apo-CaM crystal structure (PDB 1CFD). Being flexible, the B−C loop of CaM can shift in order to interact with IQ1. Side chains of residues A797 of IQ1 and N42 of CaM are evidenced to show the corresponding interaction. (B) Ribbon representation of a hypothetical model of a complex of the N-lobe Mlc1p with IQ1 based on the Mlc1p-IQ2 crystal structure (PDB 1M45). Side chains of residues A797 of IQ1 and N37 and T78 of Mlc1p are evidenced to show the short distance between A797 and N37 of the Mlc1p B−C loop. This loop in Mlc1p is rigid (N37 is hydrogen bonded to T78 of the helix D′), and consequently, a shift that would allow the interaction between IQ1 and the N-lobe of Mlc1p is less favorable.

Table 3: Growth Phenotypes Caused by Different Mutant *mlc1* Alleles

		growth[a]		
allele	mutation	25 °C	35 °C	37 °C
MLC1		+	+	+
mlc1-1	F93A	+	±	−
mlc1-8	G66S, D94G, S97N, T118N	+	+	−
mlc1-9	Y36H, T39S, I47V, D50E	+	±	−
mlc1-10	I34N, Y139C	+	±	−
mlc1-14	L59S	+	±	−
mlc1-15	I34N	+	+	+
mlc1-16	V43G	+	±	−
mlc1-17	Y139C	−[b]	n.d.[c]	n.d.

[a] To determine the growth phenotype caused by the presence of mutant *mlc1* alleles, *mlc1*Δ cells (RSY105-6A) carrying a wild type copy of *MLC1* on plasmid pRS289 (*URA3*) were transformed with a centromeric plasmid (YCp111) containing the indicated *mlc1* alleles under the control of the *MLC1* promotor. Subsequently, cells that had lost pRS289 were selected by plating on 5′-FOA-containing medium and were spotted on SC-TRP plates in order to asses the ability of the mutant *mlc1* alleles to support growth at the different temperatures. [b] No viable cells were yielded by plating *mlc1*Δ cells carrying pRS289 and YCp111-*mlc1-17* on 5′-FOA-containing medium, indicating that this *mlc1* allele is lethal. [c] n.d.: not determined.

the respective function for yeast viability. The residues I34 and Y36 are situated at the beginning and at the center of the B−C loop, respectively. Thus, the mutations I34N and Y36H (carried by the *mlc1−15* and *mlc1−9*, respectively) are likely to perturb the packaging of helix D′ within the N-loop (Figure 7D). In fact, the extra helix D′, which is a singular feature of Mlc1p, is packed toward the rest of the N-domain through the interaction of residues L75 with residues I68 (helix D) and Y36. The hydrophobic network includes also I34 and I10 located in helix A. Thus, mutation of either residue Y36 or I34, as carried by *mlc1−9* and *mlc1−15*, respectively, is expected to cause defects in the packing of helix D′ within the N-lobe leading to a different N-lobe structure and thus the dynamics of the B−C loop.

To analyze how mutations of the N-lobe affect Mlc1p function *in vivo*, the morphology of cells expressing the above-mentioned N-lobe *ts* alleles expressed from centromeric plasmids was analyzed in Δ*mlc1* cells (Figures 9B). We observed that among the mutations studied, *mlc1−9*, carrying multiple mutations within the N-lobe, produces one of the strongest cytokinesis defects (Figure 9B).

The IQGAP-like protein Iqg1p is one of the nonmyosin targets of Mlc1p. Iqg1p is the only IQGAP protein expressed in yeast cells, and it has been reported to be essential for both actomyosin ring formation and cytokinesis (*46*). Because the actomyosin ring itself is not essential for cytokinesis, Iqg1p must have other cytokinetic functions that are actomyosin ring-independent (*47*), but what this essential function might be is unknown (*46, 47*). Mlc1p acts as an Iqg1p/Cyk1p receptor at the mother-bud neck during cytokinesis shortly after spindle disassembly possibly by interacting with both Myo1p and Iqg1p (*10, 48*).

The ability of N-terminal *mlc1* mutants (*mlc1−9*, *mlc1−14*, and *mlc1−16*) to recruit GFP-tagged Iqg1p (GFP-Iqg1) at the mother-bud neck under permissive (28.0 °C) and restrictive growth conditions (37.5 °C) was determined by fluorescence microscopy (the results are summarized in Figure 9C) and compared to that of *mlc1 ts* mutants carrying amino acid substitutions solely within the C-lobe (*mlc1−1* (*8*)) or in both domains (*mlc1−8, mlc1−10*). We observed that all *mlc1* N-domain mutants tested here are affected in GFP-Iqg1p recruitment at the mother-bud neck similar to what previously observed for other *mlc1−1* and *mlc1−5* mutants that carry point mutation in the C-lobe (*9*). Among them, the point mutants *mlc1−14* and the *mlc1−16* are among those mostly affected. We concluded that the maintenance of Mlc1p N-domain structure is required for Mlc1p function *in vivo*.

In summary, the mutant *mlc1−15* solely carrying the I34N mutation can potentially affect the ability of the D′ helix to be packed in the N-lobe and, thus, to carry a destabilized B−C loop. This mutation alone does not affect Mlc1p function or yeast viability, but when it is combined with the C-terminal lethal mutation Y139C (*mlc1−17*), as is the case in the *mlc1−10 ts* mutant, restores partial function to the otherwise nonfunctional $Mlc1^{Y139C}$ protein. This data might indicate that Mlc1p N-lobe dynamics might play a functional role in those interactions in which the Mlc1p N- and C-lobes are involved. The other N-lobe Mlc1p mutants described here are likely to be more generally affected in the N-lobe structure by having different degrees of defects in the hydrophobic core that is essential for the correct packing between the two EF-hand motifs. All together, these data indicate that the myosin light chain N-lobe structure is essential for Mlc1p stability and/or interaction with partners. Moreover, our data suggest that the N-lobe rigidity might be essential for Mlc1p function *in vivo* whenever the Mlc1p is engaged in interactions that involve the C-lobe.

CONCLUSIONS

We have used ^{15}N relaxation data to extract the dynamics of the protein backbone of Mlc1p and mutagenesis analysis

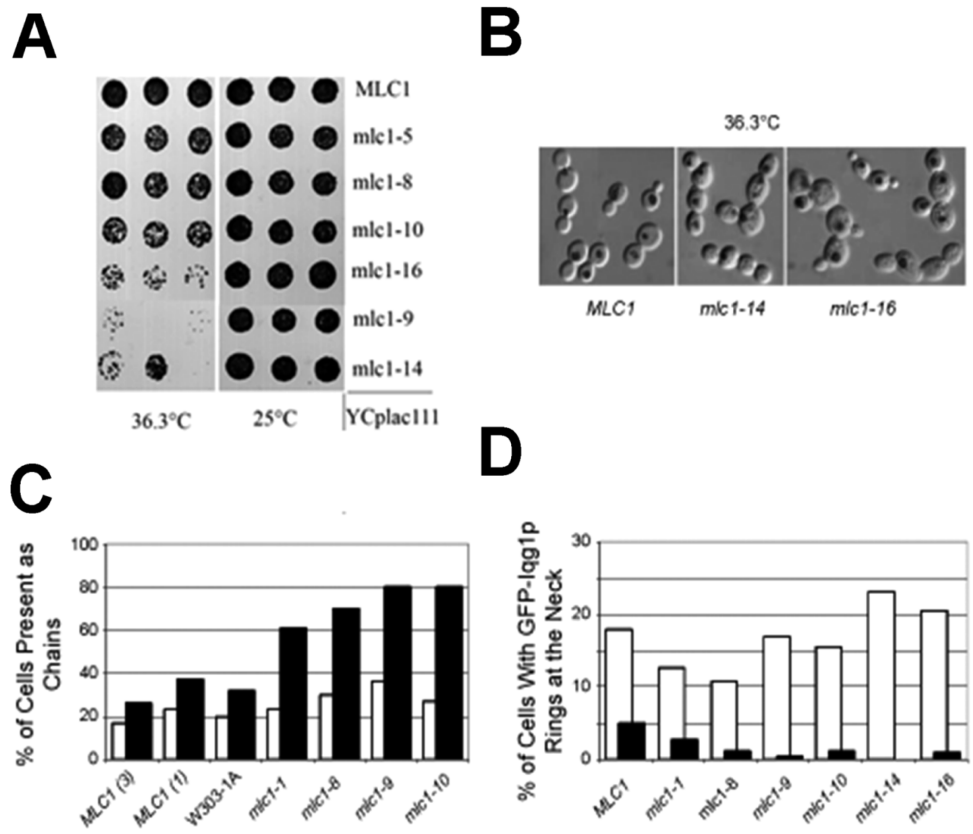

FIGURE 9: Phenotypic analysis of *mlc1* N-lobe mutant alleles. (A) A *ts* growth phenotype is caused by the indicated *mlc1* mutant alleles when expressed in the RSY105−6A cells (*mlc1*Δ). The *mlc1 ts* allele isolated from primary screenings (*9*) was cloned in the centromeric plasmid YCp111 and expressed from *MLC1* promotor in RSY105−6A cells carrying a wild type copy of *MLC1* on plasmid pRS289 (*URA3*). Subsequently, cells that had lost pRS289 were selected by plating on 5′-FOA-containing medium and were grown on SC-TRP plates for three days in order to asses the ability of the mutant *mlc1* alleles to support growth at the different temperatures. (B) The *mlc1* mutant alleles lead to the accumulation of cell chains when shifted to nonpermissive temperature. To examine cell morphology, *mlc1*Δ cells carrying centromeric plasmid YCp111 with the indicated *mlc1* alleles under control of the *MLC1* promotor, or wild type cells, were grown to logarithmic phase at 25.0 °C, before an aliquot was shifted to 36.3 °C. After 2.5 h, cells were harvested, vortexed rigorously, and examined by DIC microscopy. Panel B shows DIC images of *mlc1*Δ cells carrying YCp111 containing *MLC1*, *mlc1−14*, or *mlc1−16* at 2.5 h after the shift to 36.3 °C. The nuclei were stained with DAPI and are shown in red. The graph in panel C shows the percentage of total cells present as chains. White bars, 25.0 °C; black bars, 36.3 °C. (D) The mutant *mlc1* alleles cause defects in the recruitment of GFP-Iqg1p to the mother-bud neck. The *mlc1*Δ cells carrying the centromeric plasmid YCp111 with the indicated *mlc1* alleles were transformed with pUG35-*IQG1* and grown to logarithmic phase at 28.0 °C, before an aliquot was shifted to 37.5 °C. After 30 min, cells were harvested and examined by fluorescence microscopy. The graph shows the percentage of total cells with GFP-Iqg1p rings at the mother-bud neck; 150−200 cells for each allele were counted. White bars, 28.0 °C; black bars, 37.5 °C.

to investigate the importance of the Mlc1p N-lobe for myosin light chain function in yeast viability.

Our results show that the Mlc1p N-terminal and C-terminal domains are very different from a dynamical point of view, even though they are both constituted by two EF-hand motifs. The N-domain is much more rigid than the C-domain, which presents regions with mobility in the ps as well as μs-ms time scales. In particular, amino acids in the B−C loop and the D′ helix of the Mlc1p N-domain possess side chains that present relevant hydrophobic contacts. These interactions stabilize the N-lobe in Mlc1p, giving a higher rigidity to the Mlc1p N-terminal domain. The rigidity of the Mlc1p B−C loop and its interaction with helix D′ in the N-lobe have important consequences for the N-lobe interaction modality with target IQ peptides. The flexibility of the B−C loop of CaM compared to the rigidity of this loop in Mlc1p correlates with the different ability of the Cmd1 and Mlc1p N-domains to interact with Myo2p IQ1. It is possible for calmodulin, which presents a flexible loop, to adapt itself in order to correctly interact with the IQ1 binding site. By contrast, it is energetically very unfavorable for the Mlc1p N-domain that presents a rather rigid B−C loop and leaves, unlike calmodulin, this domain ready for interactions with a second molecular target.

Mutations within the Mlc1p N-lobe cause thermo-sensitive cytokinesis defects similar to those previously described for C-lobe mlc1 *ts* mutants (*9*). These defects appear to be due to an alteration of the N-lobe compact structure and to a defect in the ability of the mutants Mlc1p described here to interact with at least one of its targets: the Iqg1p. It has been shown recently that the intracellular levels of Iqg1p are cell-cycle regulated by ubiquitination via the anaphase promoting complex (APC/C^{Cdh1}), suggesting a function in signaling the end of anaphase, possibly in connection with Mlc1p (*47*). It will be interesting to determine whether the Mlc1p N-lobe point mutant alleles particularly affects the interaction with some but not all known Mlc1p targets. Future work will be directed toward characterizing how the Mlc1p N-lobe facilitates Mlc1p interaction with target proteins in order to clarify how the differently structured light chain N-lobe

conformation participates in the coordination of multiple protein complexes such as those controlled by Mlc1p during cytokinesis.

ACKNOWLEDGMENT

We thank Wolfgang Wagner (NIH Bethesda) for the critical reading of this manuscript, and for sharing unpublished results obtained during his Ph.D. thesis.

SUPPORTING INFORMATION AVAILABLE

The spectral density function analysis of Mlc1p from relaxation data at 1.5 mM protein concentration, pH 6.8, and 25 °C measured at 700 MHz (BMRB accession number 6332) showing residues belonging to the four regions with different dynamics characteristics. This material is available free of charge via Internet at http://pubs.acs.org.

REFERENCES

1. Trybus, K. M. (2008) Myosin V from head to tail. *Cell. Mol. Life Sci. 65*, 1378–1389.
2. Taylor, K. A. (2007) Regulation and recycling of myosin V. *Curr. Opin. Cell. Biol. 19*, 67–74.
3. Cyert, M. S. (2001) Genetic analysis of calmodulin and its targets in Saccharomyces cerevisiae. *Annu. Rev. Genet. 35*, 647–672.
4. Stevens, R. C., and Davis, T. N. (1998) Mlc1p is a light chain for the unconventional myosin Myo2p in Saccharomyces cerevisiae. *J. Cell. Biol. 142*, 711–722.
5. May, K. M., Win, T. Z., and Hyams, J. S. (1998) Yeast myosin II: a new subclass of unconventional conventional myosins? *Cell. Motil. Cytoskeleton 39*, 195–200.
6. Terrak, M., Wu, G., Stafford, W. F., Lu, R. C., and Dominguez, R. (2003) Two distinct myosin light chain structures are induced by specific variations within the bound IQ motifs-functional implications. *EMBO J. 22*, 362–371.
7. Pennestri, M., Melino, S., Contessa, G. M., Casavola, E. C., Paci, M., Ragnini-Wilson, A., and Cicero, D. O. (2007) Structural basis for the interaction of the myosin light chain Mlc1p with the myosin V Myo2p IQ motifs. *J. Biol. Chem. 282*, 667–679.
8. Desautels, M., Den Haese, J. P., Slupsky, C. M., McIntosh, L. P., and Hemmingsen, S. M. (2001) Cdc4p, a contractile ring protein essential for cytokinesis in Schizosaccharomyces pombe, interacts with a phosphatidylinositol 4 kinase. *J. Biol. Chem. 276*, 5932–5942.
9. Wagner, W., Bielli, P., Wacha, S., and Ragnini-Wilson, A. (2002) Mlc1p promotes septum closure during cytokinesis via the IQ motifs of the vesicle motor Myo2p. *EMBO J. 21*, 6397–6408.
10. Shannon, K. B., and Li, R. (2000) A myosin light chain mediates the localization of the budding yeast IQGAP-like protein during contractile ring formation. *Curr. Biol. 10*, 727–730.
11. Boyne, J. R., Yosuf, H. M., Bieganowski, P., Brenner, C., and Price, C. (2000) Yeast myosin light chain, Mlc1p, interacts with both IQGAP and class II myosin to affect cytokinesis. *J. Cell Sci. 113*, 4533–4543.
12. Terrak, M., Rebowski, G., Lu, R. C., Grabarek, Z., and Dominguez, R. (2005) Structure of the light chain-binding domain of myosin V. *Proc. Natl. Acad. Sci. U.S.A. 102*, 12718–12723.
13. Caroli-Casavola, E., Cantucci, A., Bielli, P., Di Pentima, A., Porcu, G., Pennestri, M., Cicero, D. O., and Ragnini-Wilson, A. (2008) Ypt32p and Mlc1p bind within the vesicle binding region of the class V myosin Myo2p globular tail domain. *Mol. Microbiol. 67*, 1051–1066.
14. Li, X. D., Jung, H. S., Wang, Q., Ikebe, R., Craig, R., and Ikebe, M. (2008) The globular tail domain puts on the brake to stop the ATPase cycle of myosin Va. *Proc. Natl. Acad. Sci. U.S.A. 105*, 1140–1145.
15. Weisman, L. S. (2006) Organelles on the move: insights from yeast vacuole inheritance. *Nat. Rev. Mol. Cell Biol. 7*, 243–252
16. Davis, T. N., Urdea, M. S., Masiarz, F. R., and Thorner, J. (1986) Isolation of the yeast calmodulin gene: calmodulin is an essential protein. *Cell 47*, 423–431.
17. Luan, Y., Matsuura, I., Yazawa, M., Nakamura, T., and Yagi, K. (1987) Yeast calmodulin: structural and functional differences compared with vertebrate calmodulin. *J. Biochem. 102*, 1531–1537.
18. Starovasnik, M. A., Davis, T. N., and Kevit, R. E. (1993) Similarities and differences between yeast and vertebrate calmodulin: an examination of the calcium-binding and structural properties of calmodulin from the yeast *Saccharomyces cerevisiae*. *Biochemistry 32*, 3261–3270.
19. Kay, L. E., Torchia, D. A., and Bax, A. (1989) Backbone dynamics of proteins as studied by 15N inverse detected heteronuclear NMR spectroscopy: application to staphylococcal nuclease. *Biochemistry 28*, 8972–8979.
20. Barbato, G., Ikura, M., Kay, L. E., Pastor, R. W., and Bax, A. (1992) Backbone dynamics of calmodulin studied by 15N relaxation using inverse detected two-dimensional NMR spectroscopy: the central helix is flexible. *Biochemistry 31*, 5269–5278.
21. Delaglio, F., Grzesiek, S., Vuister, G. W., Zhu, G., Pfeifer, J., and Bax, A. (1995) NMRPipe: a multidimensional spectral processing system based on UNIX pipes. *J. Biomol. NMR 6*, 277–293.
22. Johnson, B. A. (2004) Using NMRView to visualize and analyze the NMR spectra of macromolecules. *Methods Mol. Biol. 278*, 313–352.
23. Melino, S., Pennestri, M., Santoprete, A., Bielli, P., Paci, M., Ragnini-Wilson, A., and Cicero, D. O. (2005) Assignment of the 1H, 13C and 15N resonances of Mlc1p from *Saccharomices cerevisiae*. *J. Biomol. NMR 31*, 367–368.
24. Grzesiek, S., and Bax, A. (1993) The importance of not saturating water in protein NMR. Application to sensitivity enhancement and NOE measurements. *J. Am. Chem. Soc. 115*, 12593–12594.
25. Farrow, N. A., Zhang, O., Szabo, A., Torchia, D. A., and Kay, L. E. (1995) Spectral density function mapping using 15N relaxation data exclusively. *J. Biomol. NMR 6*, 153–162.
26. Lipari, G., and Szabo, A. (1982) Model Free approach to the interpretation of nuclear magnetic resonance relaxation in macromolecules. 1. Theory and range of validity. *J. Am. Chem. Soc. 104*, 4546–4559.
27. Lipari, G., and Szabo, A. (1982) Model Free approach to the interpretation of nuclear magnetic resonance relaxation in macromolecules. 2. Analysis of experimental results. *J. Am. Chem. Soc. 104*, 4559–4570.
28. Tjandra, N., Kuboniwa, H., Ren, H., and Bax, A. (1995) Rotational dynamics of calcium-free calmodulin studied by 15N-NMR relaxation measurements. *Eur. J. Biochem. 230*, 1014–1024.
29. Woessner, D. E. (1962) Nuclear spin relaxation in ellipsoids undergoing rotational brownian motion. *J. Chem. Phys. 37*, 647–654.
30. Palmer III, A. G. (2001) NMR Probes of molecular dynamics: overview and comparison with other techniques. *Annu. Rev. Biophys. Biomol. Struct. 30*, 129–155.
31. Orekhov, V. Yu, Nolde, D. E., Golovanov, A. P., Korzhnev, D. M., and Arseniev, A. S. (1995) Processing of heteronuclear NMR relaxation data with the new software DASHA. *Appl. Magn. Reson. 9*, 581–588.
32. Clore, G. M., Driscoll, P. C., Wingfield, P. T., and Gronenborn, A. M. (1990) Analysis of the backbone dynamics of interleukin-1 beta using two-dimensional inverse detected heteronuclear 15N-1H NMR spectroscopy. *Biochemistry 29*, 7387–7401.
33. Clore, G. M., Szabo, A., Bax, A., Kay, L. E., Driscoll, P. C., and Gronenborn, A. M. (1990) Deviations from the simple two-parameter model-free approach to the interpretation of nitrogen-15 nuclear magnetic relaxation of proteins. *J. Am. Chem. Soc. 112*, 4989–4991.
34. Stark, M. J. R. (1998) Studying Essential Genes-Generating and Using Promoter Fusions and Conditional Alleles, in *Yeast Gene Analysis* (Brown, A. J. P, Tuite, M., and Prosser, J., Eds.) Accademic Press Ltd., San Diego, CA.
35. Honig, B., and Nicholls, A. (1995) Classical electrostatics in biology and chemistry. *Science 268*, 1144–1149.
36. DeLano, W. L. (2002) The PyMOL Molecular Graphics System, DeLano Scientific, Palo Alto, CA (http://www.pymol.org).
37. Slupsky, C. M., Desautels, M., Huebert, T., Zhoa, R., Hemmingsen, S. M., and McIntosh, L. P. (2001) Structure of Cdc4p, a contractile ring protein essential for cytokinesis in *Schizosaccharomyces pombe*. *J. Biol. Chem. 276*, 5943–5951.
38. McCollum, D., Feoktistova, A., and Gould, K. L. (1999) Phosphorylation of the myosin-II light chain does not regulate the timing of cytokinesis in fission yeast. *J. Biol. Chem. 274*, 17691–17695.

39. Peng, J. W., and Wagner, G. (1992) Mapping of the spectral densities of N-H bond motions in eglin c using heteronuclear relaxation experiments. *Biochemistry 31*, 8571–8586.
40. Peng, J. W., and Wagner, G. (1994) Investigation of protein motions via relaxation measurements. *Methods Enzymol. 239*, 563–596.
41. Viles, J. H., Donne, D., Kroon, G., Prusiner, S. B., Cohen, F. E., Dyson, H. J., and Wright, P. E. (2001) Local structural plasticity of the prion protein. Analysis of NMR relaxation dynamics. *Biochemistry 40*, 2743–2753.
42. Escobar-Cabrera, E., Venkatesan, M., Desautels, M., Hemmingsen, S. M., and McIntosh, L. P. (2005) Dissecting the domain structure of Cdc4p, a myosin essential light chain involved in *Schizosaccharomyces pombe* cytokinesis. *Biochemistry 44*, 12136–12148.
43. Peng, J. W., and Wagner, G. (1995) Frequency spectrum of NH bonds in eglin c from spectral density mapping at multiple fields. *Biochemistry 34*, 16733–16752.
44. Stone, M. J. (2001) NMR relaxation studies of the role of conformational entropy in protein stability and ligand binding. *Acc. Chem. Res. 34*, 379–388.
45. Pawley, N. H., Gans, J. D., and Nicholson, L. K. (2002) Factors determining the reliable description of global tumbling parameters in solution NMR. *J. Biomol. NMR 24*, 215–229.
46. Shannon, K. B., and Li, R. (1999) The multiple roles of Cyk1p in the assembly and function of the actomyosin ring in budding yeast. *Mol. Biol. Cell 10*, 283–296.
47. Ko, N., Nishihama, R., Tully, G. H., Ostapenko, D., Solomon, M. J., Morgan, D. O., and Pringle, J. R. (2007) Identification of yeast IQGAP (Iqg1p) as an anaphase-promoting-complex substrate and its role in actomyosin-ring-independent cytokinesis. *Mol. Biol. Cell 18*, 5139–5153.
48. Tolliday, N., Pitcher, M., and Li, R. (2003) Direct evidence for a critical role of myosin II in budding yeast cytokinesis and the evolvability of new cytokinetic mechanisms in the absence of myosin II. *Mol. Biol. Cell 14*, 798–809.

BI801178T